

# Numerical Hopf–Lax formulae for Hamilton–Jacobi equations on unstructured geometries

S. Cacace\*, R. Ferretti†, G. Tatafiore‡

March 18, 2025

## Abstract

We consider a scheme of Semi-Lagrangian (SL) type for the numerical solution of Hamilton–Jacobi (HJ) equation on unstructured triangular grids. As it is well known, SL schemes are not well suited for unstructured grids, due to the cost of the point location phase; this drawback is augmented by the need for repeated minimization. In this work, we propose a scheme that works only on the basis of node values and connectivity of the grid. In a first version, we obtain a monotone scheme; then, applying a quadratic refinement to the numerical solution, we improve accuracy at the price of some extra computational cost. The scheme can be applied to both time-dependent and stationary HJ equations; in the latter case, we also study the construction of a fast policy iteration solver. We perform a theoretical analysis of the two versions, and validate them with an extensive set of examples, both in the time-dependent and in the stationary case.

## 1 Introduction

Born in the 1950s in the framework of environmental fluid dynamics, semi-Lagrangian (SL) schemes are typically used to approximate hyperbolic equations, or advection terms in more complex evolution operators, using characteristics in numerical form. The simplest case is that of the constant-coefficient advection equation

$$\begin{cases} u_t + a \cdot Du = 0 & (x, t) \in \mathbb{R}^d \times \mathbb{R}^+, \\ u(x, 0) = u_0(x), \end{cases}$$

where the vector  $a \in \mathbb{R}^d$  is the advection speed and  $Du$  denotes the gradient of the function  $u$ . In this case, the solution may be represented by the well-known formula

$$u(x, t) = u_0(x - at), \tag{1}$$

---

\*Dipartimento di Matematica, “Sapienza” Università di Roma, P.le Aldo Moro, 1, Roma, Italy; [simone.cacace@uniroma1.it](mailto:simone.cacace@uniroma1.it)

†Dipartimento di Matematica e Fisica, Università Roma Tre, Largo S. Leonardo Murialdo, 1, Roma, Italy; [roberto.ferretti@uniroma3.it](mailto:roberto.ferretti@uniroma3.it)

‡Dipartimento di Matematica, “Sapienza” Università di Roma, P.le Aldo Moro, 1, Roma, Italy; [giulia.tatafiore@uniroma1.it](mailto:giulia.tatafiore@uniroma1.it)

which is in turn discretized in SL form as

$$v_j^{n+1} = I[V^n](x_j - a\Delta t). \quad (2)$$

In (2),  $I[V](x)$  represents an interpolation operator based on the values  $v_i$  of the vector  $V$  (associated to a space grid of nodes  $x_i$ ), computed at the point  $x$ . Moreover, given a time discretization of step  $\Delta t$ , the notation  $v_j^n$  stands for an approximation of the solution at the node  $x_j$  and time  $t_n = n\Delta t$ , and  $V^n$  stands for the vector collecting all such values.

Our interest here is towards the Hamilton–Jacobi (HJ) equation

$$\begin{cases} u_t + H(Du) = 0 & (x, t) \in \mathbb{R}^d \times \mathbb{R}^+, \\ u(x, 0) = u_0(x), \end{cases} \quad (3)$$

with a strictly convex Hamiltonian  $H$ . In this case, the characteristic-based representation formula (1) admits a nonlinear generalization, namely the following *Hopf–Lax formula*

$$u(x, t) = \inf_{y \in \mathbb{R}^d} \left\{ u_0(y) + tH^* \left( \frac{x - y}{t} \right) \right\}, \quad (4)$$

where  $H^*$  is the Legendre transform of  $H$ , defined as

$$H^*(q) = \sup_{p \in \mathbb{R}^d} \{p \cdot q - H(p)\}.$$

We recall that, if  $H$  is *strongly coercive*, that is, if

$$\lim_{|p| \rightarrow \infty} \frac{H(p)}{|p|} = +\infty,$$

then  $H^*$  is also well defined, strictly convex and strongly coercive.

The similarity between (4) and (1) is more apparent if we set  $a = (x - y)/t$ , and (4) is recast in the form

$$u(x, t) = \inf_{a \in \mathbb{R}^d} \{u_0(x - at) + tH^*(a)\}, \quad (5)$$

which has been widely used for the SL discretization of (3), as well as of the Bellman equation of Dynamic Programming (see [6, 7] and the references therein). For (5), the SL discretization has the structure

$$v_j^{n+1} = \min_{a \in \mathbb{R}^d} \{I[V^n](x - a\Delta t) + \Delta tH^*(a)\}, \quad (6)$$

and implies two steps, crucial for efficiency: interpolation and minimization. In this formulation of the scheme, efficiency may have a serious drop when using unstructured grids, due to the complexity of locating the point  $x - a\Delta t$  on the space triangulation, a phase to be repeated at each computation of the function to be minimized.

In this work, we will discretize again the representation formula (4) to obtain an approximation scheme for (3). However, in order to improve efficiency on the unstructured geometries to which this work is ultimately directed, we will drop the interpolation phase

and perform minimization with a walk on the space grid, much in the spirit of [4]. We will then adapt this technique to the stationary case

$$\lambda u + H(Du) = f(x) \quad x \in \mathbb{R}^d, \quad (7)$$

focusing in particular on a fast solver based on Policy Iteration (PI).

The outline of the paper is as follows. In Section 2 we will construct the scheme in the evolutive case and prove its convergence on the basis of the Barles–Souganidis theory [1], while Section 3 retraces the construction of the scheme for the stationary case (7). Last, we present a numerical validation in Section 6, and draw some conclusions in Section 7.

## 2 Construction of the scheme, time-dependent case

We start by listing the minimal assumptions on the problem (3).

### Basic assumptions

- $H(\cdot)$  is  $C^2$  with bounded second derivatives, strictly convex and strongly coercive;
- $u_0$  is bounded and uniformly continuous.

We recall that, under these assumptions, a unique solution of (3) exists in the viscosity sense. For any  $t > 0$ , the solution is also semiconcave, that is, it satisfies a unilateral upper bound on the second incremental ratios (see [7]).

In the numerical approximation, we assume that the space grid covers the whole of  $\mathbb{R}^d$ . We will denote by  $v_j^n$  the approximation of the solution at the node  $x_j$  and time  $t_n = n\Delta t$  (for  $j \in \mathbb{N}$  and  $n \geq 0$ ), and  $V^n$  will stand for the infinite vector collecting all such values (we will later consider the equation on a bounded domain  $\Omega$  with Dirichlet boundary conditions). We will avoid any assumption on both the regularity of the grid and the shape of the elements (although in the numerical examples they will be taken as triangles). We will also denote by  $\Delta x$  the maximum diameter of the grid elements.

### 2.1 Restricting the Hopf–Lax formula to nodes

We start by rewriting the Hopf–Lax formula (4) on a single time step, from  $t_n$  to  $t_{n+1}$ :

$$u(x, t_{n+1}) = \inf_{y \in \mathbb{R}^d} \left\{ u(y, t_n) + \Delta t H^* \left( \frac{x - y}{\Delta t} \right) \right\}. \quad (8)$$

We note that, due to the strong coercivity of  $H$  and boundedness of  $u_0$ , the inf operator can be replaced by a min. Indeed, since the function

$$f(y) = u_0(y) + t H^* \left( \frac{x - y}{t} \right)$$

is continuous and coercive, there exists a minimum point  $\bar{y}$  for every  $x \in \mathbb{R}^d$ ,  $t \in \mathbb{R}^+$ . Moreover, given the basic assumptions above, the search for the minimum point can be confined to a compact set, as proved in [6].

Then, we restrict the computation to nodes, obtaining the fully discrete version

$$\begin{cases} v_j^{n+1} = \min_{k \in \mathbb{N}} \left\{ v_k^n + \Delta t H^* \left( \frac{x_j - x_k}{\Delta t} \right) \right\}, \\ v_j^0 = u_0(x_j). \end{cases} \quad (9)$$

In previous works (see, e.g., [6]), the discretization of (8) has been carried out by taking  $y \in \mathbb{R}^d$  and using a descent-type minimization algorithm, with an interpolated value for  $u(y, t_n)$ . In this case, at the price of some drop in accuracy, we avoid both phases of interpolation and iterative minimization, which would result in a high computational cost. We remark that this use of the Hopf–Lax formula has some precedent (for example, [3]), although, to the Authors’ knowledge, no attempt to optimize the algorithm for unstructured grids has been made so far.

Convergence of this scheme will be analysed now in the framework of Barles–Souganidis theory [1]. As it is well-known, this convergence theory requires the scheme to be monotone,  $L^\infty$ -stable and consistent. In our case, the scheme is invariant for the addition of constants, since, for any  $c \in \mathbb{R}$ ,

$$\min_{k \in \mathbb{N}} \left\{ (v_k^n + c) + \Delta t H^* \left( \frac{x_j - x_k}{\Delta t} \right) \right\} = \min_{k \in \mathbb{N}} \left\{ v_k^n + \Delta t H^* \left( \frac{x_j - x_k}{\Delta t} \right) \right\} + c,$$

so that  $L^\infty$  stability may be deduced from monotonicity via the results in [5].

### Monotonicity and $L^\infty$ stability

Assume now that  $V$  and  $W$  are two vectors of nodal values such that  $V \geq W$  element by element. We want to prove that

$$\min_{k \in \mathbb{N}} \left\{ v_k + \Delta t H^* \left( \frac{x_j - x_k}{\Delta t} \right) \right\} \geq \min_{m \in \mathbb{N}} \left\{ w_m + \Delta t H^* \left( \frac{x_j - x_m}{\Delta t} \right) \right\}. \quad (10)$$

Let the indices achieving the minimum on the left- and right-hand side of (10) be denoted, respectively, by  $k^*$  and  $m^*$ . Then, (10) may be rewritten as

$$v_{k^*} + \Delta t H^* \left( \frac{x_j - x_{k^*}}{\Delta t} \right) \geq w_{m^*} + \Delta t H^* \left( \frac{x_j - x_{m^*}}{\Delta t} \right).$$

On the other hand,  $m^*$  achieves the minimum, and this implies that

$$w_{k^*} + \Delta t H^* \left( \frac{x_j - x_{k^*}}{\Delta t} \right) \geq w_{m^*} + \Delta t H^* \left( \frac{x_j - x_{m^*}}{\Delta t} \right), \quad (11)$$

but, since  $V \geq W$ , we also have that

$$v_{k^*} + \Delta t H^* \left( \frac{x_j - x_{k^*}}{\Delta t} \right) \geq w_{k^*} + \Delta t H^* \left( \frac{x_j - x_{k^*}}{\Delta t} \right).$$

Then, using (11), we obtain a fortiori that (10) is satisfied. The scheme (9) is therefore monotone and  $L^\infty$  stable.

## Consistency

Let now  $u$  be a smooth solution of (3). Consistency of the scheme requires that for all  $j$ , as  $\Delta x, \Delta t \rightarrow 0$ ,

$$L(x_j, \Delta x, \Delta t) = \frac{1}{\Delta t} \left( u(x_j, t_{n+1}) - \min_{k \in \mathbb{N}} \left\{ u(x_k, t_n) + \Delta t H^* \left( \frac{x_j - x_k}{\Delta t} \right) \right\} \right) \rightarrow 0. \quad (12)$$

Rewriting now  $u(x_j, t_{n+1})$  via (8), we get

$$\begin{aligned} L(x_j, \Delta x, \Delta t) &= \frac{1}{\Delta t} \left( \min_{y \in \mathbb{R}^d} \left\{ u(y, t_n) + \Delta t H^* \left( \frac{x_j - y}{\Delta t} \right) \right\} \right. \\ &\quad \left. - \min_{k \in \mathbb{N}} \left\{ u(x_k, t_n) + \Delta t H^* \left( \frac{x_j - x_k}{\Delta t} \right) \right\} \right). \end{aligned} \quad (13)$$

We therefore have to estimate the difference between the minimum of the smooth function

$$\mathcal{F}_j(y) = u(y, t_n) + \Delta t H^* \left( \frac{x_j - y}{\Delta t} \right) \quad (14)$$

and its minimum restricted to a grid with step  $\Delta x$ ; for simplicity, we will carry out the computation in one space dimension.

Since at the minimum point  $\bar{y}$  we have  $\mathcal{F}'_j(\bar{y}) = 0$ , the difference  $\mathcal{F}_j(x_k) - \mathcal{F}_j(\bar{y})$ , for  $x_k - \bar{y} = O(\Delta x)$ , may be estimated via a Taylor expansion centred at  $\bar{y}$  as

$$\mathcal{F}_j(x_k) - \mathcal{F}_j(\bar{y}) = \frac{\mathcal{F}''_j(\eta)}{2} (x_k - \bar{y})^2 \leq \frac{\|\mathcal{F}''_j\|_\infty}{2} \Delta x^2$$

This requires to give an upper bound on the second derivative of  $\mathcal{F}_j$ . We have

$$\mathcal{F}''_j(y) = u_{xx}(y, t_n) + \Delta t \frac{1}{\Delta t^2} H^{*''} \left( \frac{x_j - y}{\Delta t} \right).$$

The first term in the right-hand side is bounded for a smooth solution, while the second, given the boundedness of  $H^{*''}$ , is of order  $1/\Delta t$ . Then, the difference between the minimum of  $\mathcal{F}_j$  and its minimum value at the nodes is  $O(\|H^{*''}\|_\infty \Delta x^2)$ , and the consistency error turns out to be

$$L(x_j, \Delta x, \Delta t) = \frac{1}{\Delta t} O \left( \frac{\Delta x^2}{\Delta t} \right) = O \left( \frac{\Delta x^2}{\Delta t^2} \right).$$

Therefore, the scheme is consistent under an inverse CFL condition  $\Delta x = o(\Delta t)$ . For example, taking the relationship  $\Delta t \sim \Delta x^{1/2}$ , the scheme turns out to be first-order w.r.t.  $\Delta x$ .

We can finally summarize this convergence analysis in the following

**Theorem 1** *Let the basic assumptions hold, and assume in addition that  $\Delta x = o(\Delta t)$ . Then, the numerical solution  $V^n$  defined by (9) converges to the solution  $u(x, t_n)$  of (3) locally uniformly on  $\mathbb{R}^d \times [0, T]$  as  $\Delta t, \Delta x \rightarrow 0$  for any  $T > 0$ .*

**Remark 1** *In case weak Dirichlet conditions (see [7]) are enforced in (3), assume that the boundary datum  $b_j = b(x_j)$  is assigned at a boundary node  $x_j$  for a given function  $b$ . Then, the update formula (9) for  $v_j$  is replaced by*

$$v_j^{n+1} = \min \left\{ b_j, \min_k \left\{ v_k^n + \Delta t H^* \left( \frac{x_j - x_k}{\Delta t} \right) \right\} \right\}.$$

*In the dynamic programming setting, this amounts to set a stopping cost on the boundary of the domain. The above convergence analysis can be replicated with minor modifications.*

### 3 Construction of the scheme, stationary case

We turn now to the stationary equation (7). In the time-marching framework, its solution can be seen as the asymptotic solution, for  $t \rightarrow \infty$ , of the time-dependent equation

$$\begin{cases} u_t + \lambda u + H(Du) = f(x) & (x, t) \in \mathbb{R}^d \times \mathbb{R}^+, \\ u(x, 0) = u_0(x). \end{cases} \quad (15)$$

On the other hand, using Dynamic Programming arguments (see [7]), it is possible to prove that the solution of (7) (or, in other terms, the regime solution of (15)) satisfies

$$u(x) = \inf_{\alpha \in \mathcal{A}} \left\{ e^{-\lambda \Delta t} u(y(\Delta t; \alpha)) + \int_0^{\Delta t} \left( f(y(s; \alpha)) + H^*(\alpha(s)) \right) e^{-\lambda s} ds \right\}, \quad (16)$$

where  $\mathcal{A}$  stands for the set of measurable functions mapping  $[0, +\infty]$  into  $\mathbb{R}^d$ , and  $y(s; \alpha)$  solves the ODE system

$$\begin{cases} \dot{y}(s; \alpha) = \alpha(s), & s > 0 \\ y(0, \alpha) = x. \end{cases}$$

In view of the  $x$ -dependence of  $f$ , (16) cannot be given by an exact Hopf–Lax type form; therefore, setting  $y = y(\Delta t; \alpha)$ , and  $\alpha(s) \equiv (x - y)/\Delta t$ , and assuming smoothness as usual, we approximate the integral in (16) as

$$\int_0^{\Delta t} \left( f(y(s; \alpha)) + H^*(\alpha(s)) \right) e^{-\lambda s} ds = \Delta t \left( f(x) + H^* \left( \frac{x - y}{\Delta t} \right) \right) + O(\Delta t^2). \quad (17)$$

With this approximation, (16) is in turn approximated as

$$w(x) = \min_{y \in \mathbb{R}^d} \left\{ e^{-\lambda \Delta t} w(y) + \Delta t H^* \left( \frac{x - y}{\Delta t} \right) \right\} + \Delta t f(x). \quad (18)$$

In a second discretization step, according to what has been done for the time-dependent case, we restrict both the computation and the minimum search to the set of grid nodes, obtaining

$$v_j = \min_{k \in \mathbb{N}} \left\{ e^{-\lambda \Delta t} v_k + \Delta t H^* \left( \frac{x_j - x_k}{\Delta t} \right) \right\} + \Delta t f(x_j), \quad (19)$$

with obvious modifications in the case of Dirichlet boundary conditions.

Equation (19) is a fixed-point equation, and it is easy to show that it has a contractive right-hand side (see [7]); this ensures that it has a unique solution  $V$ . As for the convergence of  $V$  to the solution of (7), it is possible to retrace the arguments in [7], along with those of the time-dependent case above, to obtain a consistency estimate in the form

$$L(x_j, \Delta x, \Delta t) = \frac{1}{\Delta t} \left( O\left(\frac{\Delta x^2}{\Delta t}\right) + O(\Delta t^2) \right) = O\left(\frac{\Delta x^2}{\Delta t^2}\right) + O(\Delta t). \quad (20)$$

and then the following

**Theorem 2** *Let the basic assumptions hold, and assume in addition that  $\Delta x = o(\Delta t)$ . Then, the numerical solution  $V^n$  defined by (19) converges to the solution  $u(x, t_n)$  of (7) locally uniformly on  $\mathbb{R}^d$  as  $\Delta t, \Delta x \rightarrow 0$ .*

While approximating the integral as in (17) suffices to obtain a consistent scheme for  $\Delta x = o(\Delta t)$ , the term  $O(\Delta t)$  becomes a bottleneck for the consistency rate. An easy computation shows that the truncation error (20) is maximized taking  $\Delta t \sim \Delta x^{2/3}$ , and accordingly the consistency rate w.r.t.  $\Delta x$  drops to 2/3. A way to increase the rate is to approximate the integral of  $f$  by a trapezoidal quadrature rule,

$$\int_0^{\Delta t} f(y(s; \alpha)) e^{-\lambda s} ds = \Delta t \frac{f(x) + e^{-\lambda \Delta t} f(y)}{2} + O(\Delta t^3), \quad (21)$$

which results in the scheme

$$v_j = \min_{k \in \mathbb{N}} \left\{ e^{-\lambda \Delta t} v_k + \Delta t H^* \left( \frac{x_j - x_k}{\Delta t} \right) + \frac{\Delta t}{2} e^{-\lambda \Delta t} f(x_k) \right\} + \frac{\Delta t}{2} f(x_j). \quad (22)$$

In this case, given the increase of the approximation order for the integral of  $f$ , the consistency error reads

$$L(x_j, \Delta x, \Delta t) = \frac{1}{\Delta t} \left( O\left(\frac{\Delta x^2}{\Delta t}\right) + O(\Delta t^3) \right) = O\left(\frac{\Delta x^2}{\Delta t^2}\right) + O(\Delta t^2), \quad (23)$$

the consistency rate is maximized under the relationship  $\Delta t \sim \Delta x^{1/2}$  and its optimal value is 1.

### 3.1 Value iteration

In the easiest approach, (19) may be solved by the so-called *value iteration*, that is, via the iteration

$$v_j^{(n+1)} = \min_{k \in \mathbb{N}} \left\{ e^{-\lambda \Delta t} v_k^{(n)} + \Delta t H^* \left( \frac{x_j - x_k}{\Delta t} \right) \right\} + \Delta t f(x_j), \quad (24)$$

where the index  $n$  should now be understood as an iteration number (an obvious modification applies for treating (22)). Since the right-hand side of (19) is a contraction, the iteration (24) converges to its unique fixed point. The contraction coefficient, however, is given by  $e^{-\lambda \Delta t}$ , and the convergence becomes very slow as the approximation is refined. This backs the use of faster solvers for the fixed-point equation, in particular the so-called *Policy Iteration* (PI), which will be briefly reviewed here.

### 3.2 Exact policy iteration

For a problem with  $N$  unknowns (in our case, with a grid of  $N$  nodes), the standard matrix form of the Policy Iteration algorithm reads

$$\min_{\alpha \in U^N} (B(\alpha)V - c(\alpha)) = 0, \quad (25)$$

in which  $B$  is a square  $N \times N$  matrix,  $V \in \mathbb{R}^N$  is the vector of the discretized solution, and  $c \in \mathbb{R}^N$  is the vector of costs. After setting  $n = 0$  and choosing an initial policy  $\alpha^{(0)}$ , the PI evolves by alternating the two phases

1. *Policy evaluation:*  $V^{(n)}$  is computed as the solution of the linear system

$$B(\alpha^{(n)})V^{(n)} = c(\alpha^{(n)}),$$

2. *Policy improvement:* a new policy  $\alpha^{(n+1)}$  is set as

$$\alpha^{(n+1)} = \arg \min_{\alpha \in U^N} (B(\alpha)V^{(n)} - c(\alpha)),$$

until a suitable convergence condition is satisfied.

Among the wide literature on policy iteration, we quote here the pioneering theoretical analysis of Puterman and Brumelle [8], which have shown that the linearization procedure underlying policy iteration is conceptually equivalent to a Newton-type iterative solver. More recently, this result has been further generalized in [2] in the following superlinear convergence result:

**Theorem 3 ([2])** *Assume that:*

**(P1)** *The functions  $B : U^N \rightarrow \mathbb{R}^{N \times N}$  and  $c : U^N \rightarrow \mathbb{R}^N$  are continuous.*

**(P2)** *For every  $\alpha \in U^N$ , the matrix  $B(\alpha)$  is monotone, that is,  $B(\alpha)$  is invertible and  $B^{-1}(\alpha) \geq 0$  elementwise.*

*Then, there exists a unique  $V$  solution of (25). Moreover, the sequence  $V^{(n)}$  generated by the PI algorithm satisfies the following:*

1.  $V^{(n+1)} \leq V^{(n)}$  for every  $n \geq 0$ ;
2.  $V^{(n)} \rightarrow V$  as  $n \rightarrow +\infty$ , for every initial policy  $\alpha_0$ ;
3.  $\|V^{(n+1)} - V\| = o(\|V^{(n)} - V\|)$  as  $n \rightarrow +\infty$ .

In the case of the discretization (19), we can recast the scheme in the form

$$\min_{k \in \mathbb{N}} \left\{ -v_j + e^{-\lambda \Delta t} v_k + \Delta t \left( H^* \left( \frac{x_j - x_k}{\Delta t} \right) + f(x_j) \right) \right\} = 0. \quad (26)$$

To interpret (26) in the form (25), it suffices to define the elements of the matrix  $B(k)$  and the vector  $c(k)$  as

$$b_{jm}(k) = \begin{cases} 1 & \text{if } m = j \neq k \\ -e^{-\lambda\Delta t} & \text{if } m = k \neq j \\ 1 - e^{-\lambda\Delta t} & \text{if } m = j = k \\ 0 & \text{otherwise;} \end{cases} \quad c_j(k) = \Delta t \left( H^* \left( \frac{x_j - x_k}{\Delta t} \right) + f(x_j) \right). \quad (27)$$

In this case, denoting by  $k_j$  the node index achieving the minimum in (26), and changing all the signs, the policy evaluation phase is rewritten as the system

$$v_j - e^{-\lambda\Delta t} v_{k_j} = \Delta t \left( H^* \left( \frac{x_j - x_{k_j}}{\Delta t} \right) + f(x_j) \right) \quad (j = 1, \dots, N). \quad (28)$$

With these definitions, assumptions **(P1)**–**(P2)** of Theorem 3 are satisfied. In fact, the continuity of  $B$  and  $c$  is obvious once the set of node indices is naturally endowed with the discrete topology. As for **(P2)**, we note that an equivalent definition of monotone matrix requires the off-diagonal elements to be nonpositive (which is clearly the case), and the eigenvalues to have nonnegative real part; this latter property is true, as a consequence of Gershgorin’s theorem. Note that monotonicity of the matrices  $B$  implies their nonsingularity, and thus the unique solvability of the policy evaluation phase.

Clearly, the form (22) of the scheme can be treated by changing the definition of the vector  $c(k)$  into

$$c_j(k) = \Delta t \left( H^* \left( \frac{x_j - x_k}{\Delta t} \right) + \frac{f(x_j) + e^{-\lambda\Delta t} f(x_k)}{2} \right),$$

and the policy evaluation step is changed accordingly.

### 3.3 Modified policy iteration

An adaptation of policy iteration to large sparse problems has been proposed as “modified policy iteration” (MPI) in [9], and has also become a classical tool. In this case, the policy evaluation phase is carried out in iterative form, which may be convenient in very large problems, whenever a direct solver would be unfeasible. In the specific case of (26), once given an initial guess for the policy, the two phases of MPI can be written as

1. *Policy evaluation:*  $V^{(n)}$  is computed by iterating on  $m$  the update formula

$$v_{j,m+1}^{(n)} = e^{-\lambda\Delta t} v_{k_j^{(n)},m}^{(n)} + \Delta t \left( H^* \left( \frac{x_j - x_{k_j^{(n)}}}{\Delta t} \right) + f(x_j) \right)$$

up to a given stopping condition;

2. *Policy improvement:* a new policy  $k_j^{(n+1)}$  is set as

$$k_j^{(n+1)} = \arg \min_{k \in \mathbb{N}} \left\{ -v_j^{(n)} + e^{-\lambda\Delta t} v_k^{(n)} + \Delta t \left( H^* \left( \frac{x_j - x_k}{\Delta t} \right) + f(x_j) \right) \right\}.$$

Here, we have denoted by  $v_{j,m}^{(n)}$  the  $j$ -th element of the  $m$ -th iterate in the policy evaluation, by  $v_j^{(n)}$  the corresponding final value of the iteration (i.e., the  $j$ -th element of  $V^{(n)}$ ), and by  $k_j^{(n)}$  the  $j$ -th element of the optimal policy at the  $n$ -th iteration.

**Remark 2** *Since the policy is defined, in this scheme, by the set of indices  $k_j$  of the nodes achieving the minima for  $\mathcal{F}_j$ , we can consider the policy to be convergent as soon as none of these indices is any longer updated.*

## 4 Unstructured implementation

We provide some details for the actual implementation of the fully discrete scheme under consideration, on two-dimensional triangular grids. The aim is to compute the global minimum in (9) as efficiently as possible, in terms of both space and time complexity, by means of walks along the grid nodes that locally decrease the right hand side of our scheme. To this end, once a triangulation (typically, Delaunay) is given, we only assume to work with the minimal data structures describing the domain geometry, namely vertex and triangle lists, plus a connectivity list which contains, for each triangle, the indices of its first triangle neighbors along its three edges. More precisely, we denote by  $\mathcal{X} = \{x_j\}_{j=1,\dots,|\mathcal{X}|}$  the list of vertex coordinates  $x_j \in \mathbb{R}^2$  where  $|\mathcal{X}|$  is the total number of vertices, by  $\mathcal{T} = \{T_j = (j_1, j_2, j_3)\}_{j=1,\dots,|\mathcal{T}|}$  the list of index triplets defining the  $j$ -th triangle with vertices  $x_{j_1}, x_{j_2}, x_{j_3}$  where  $|\mathcal{T}|$  is the total number of triangles, and by  $\mathcal{TN} = \{TN_j = (j_1, j_2, j_3)\}_{j=1,\dots,|\mathcal{T}|}$  the list of index triplets corresponding to the three neighbors  $T_{j_1}, T_{j_2}, T_{j_3}$ , of the  $j$ -th triangle (for boundary elements one or two indices are set to zero if the corresponding neighbors are missing). Note that, in order to walk on the grid along the vertices, using  $\mathcal{TN}$  is much cheaper than storing the first neighbors of each vertex, since the number of neighbors per vertex typically ranges from four up to eleven. Here we just store three indices per triangle, and we can use this connectivity list to move around a vertex, and accomplish the same task of finding vertex neighbors in constant time, by means of a custom function `vertex_neighbors`.

Now, the crucial point of our minimization procedure is the initialization of each walk. It is well known that the solutions of (3) can develop gradient discontinuities (shocks) that, while moving in time, can change completely the domain of dependence of the solution itself. At the discrete level this implies that the grid node achieving the global minimum in (9) can suddenly change from one time step to the next, hence that some walk can be trapped in a local minimum. As a workaround to this scenario, we propose a simple but still effective procedure to handle nonsmooth solutions. The idea is to run, for each grid node  $x_j$ , different walks starting from a batch of neighboring nodes within a circle of radius proportional to  $\Delta t$ , in order to climb possible discontinuities and drive at least one walk to the correct minimum. In two dimensions, a reasonable compromise in terms of computational efforts is to use four points, obtained by displacing  $x_j$  along coordinate axis, two per dimension in opposite directions, and accepting as correct the best of the values obtained by the four walks. More precisely, given a constant  $C > 0$ , we consider the four directions  $e_1 = (1, 0), e_2 = (-1, 0), e_3 = (0, 1), e_4 = (0, -1)$  and the four displacements of

each grid node  $x_j$  for  $j = 1, \dots, |\mathcal{X}|$ :

$$x_{j,d} = x_j + C\Delta t e_d \quad \text{for } d = 1, \dots, 4. \quad (29)$$

Denoting by

$$k_{j,d} = \arg \min_{k=1, \dots, |\mathcal{X}|} |x_{j,d} - x_k|$$

the index of the closest vertex projection of  $x_{j,d}$  on the grid, we build the index displacement lists  $\mathcal{K}^d$  by setting  $\mathcal{K}_j^d = k_{j,d}$  for  $d = 1, \dots, 4$  and  $j = 1, \dots, |\mathcal{X}|$ .

This yields the following descent algorithm for the computation of the proposed node-restricted Hopf–Lax formula, presented in Algorithm 1.

---

**Algorithm 1** Node\_Restricted\_HL

---

```

1: Given  $\mathcal{X}, \mathcal{T}, \mathcal{TN}, \Delta t, N, u_0, H^*, b$ 
2:  $v_j^0 \leftarrow u_0(x_j)$  for  $j = 1, \dots, |\mathcal{X}|$ .
3: for  $n = 0 : N$  do
4:   for  $j = 1 : |\mathcal{X}|$  do
5:     for  $d = 1 : 4$  do
6:       WALK  $\leftarrow$  true
7:        $k_{\text{old}} \leftarrow \mathcal{K}_j^d$ 
8:       while WALK do
9:          $\mathcal{N} \leftarrow \{k_{\text{old}}\} \cup \text{vertex\_neighbors}(k_{\text{old}})$ 
10:         $k_{\text{new}} \leftarrow \arg \min_{k \in \mathcal{N}} \mathcal{F}(k), \quad \mathcal{F}(k) = \left\{ v_k^n + \Delta t H^* \left( \frac{x_j - x_k}{\Delta t} \right) \right\}$ 
11:        WALK  $\leftarrow$  ( $k_{\text{new}} \neq k_{\text{old}}$ )
12:         $k_{\text{old}} \leftarrow k_{\text{new}}$ 
13:      end while
14:       $v_{j,d} \leftarrow \mathcal{F}(k_{\text{new}})$ 
15:    end for
16:    if  $x_j$  on the boundary then
17:       $v_j^{n+1} \leftarrow \min \{b_j, \min_{d=1, \dots, 4} v_{j,d}\}$ 
18:    else
19:       $v_j^{n+1} \leftarrow \min_{d=1, \dots, 4} v_{j,d}$ 
20:    end if
21:  end for
22: end for

```

---

We remark that, under the assumption that the solution is convex, we can completely remove the initialization of walks based on different seeds. Actually, in such cases,  $\mathcal{F}$  is also convex and has a unique global minimum. In this setting, inspired by [4], we can further optimize the process by starting the walk from the node that attained the minimum in the previous time step, and this leads to a significant speed-up in the overall computation.

We finally observe that, since we are interested in walks that strictly decrease  $\mathcal{F}$ , the function `vertex_neighbors` can be combined with an index-based comparison to restrict the evaluation of  $\mathcal{F}$  only to the vertices that have not already been visited. This can clearly mitigate the overall computational cost of the algorithm in case the computation of  $\mathcal{F}$  is particularly expensive.

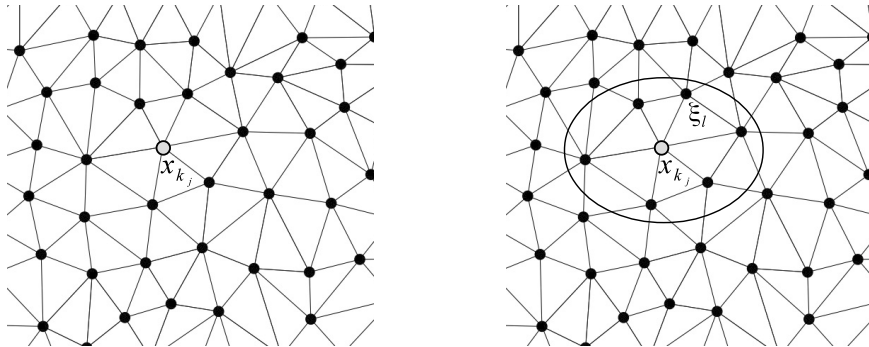


Figure 1: Node achieving the minimum in (9) (left) and related stencil for quadratic refinement (right).

The implementation of the proposed schemes for the stationary equation (7) on triangular grids parallels the one for the evolutive case presented in Section 2. In particular, we have to take into account the new terms related to the discount factor  $\lambda$  and the source  $f$  appearing in the right-hand side of (19). Moreover, for the value iteration scheme (24) we can readily apply Algorithm 1, just reinterpreting the number of time steps as the number of fixed-point iterations, and adding a stopping criterion based on some norm of the difference between two successive iterations. On the other hand, for both exact and modified policy iteration schemes, we have to embed our vertex neighbors minimum search in the policy improvement phase.

## 5 Quadratic refinement of the minimum search

One major drawback of the scheme in the form (9) is the relatively low accuracy. We propose therefore a more accurate version, still working without a numerical minimization phase, which will be sketched for simplicity in two space dimensions. In this version, the refinement of the minimum search is performed via a local quadratic approximation.

Let  $\mathcal{F}_j(y)$  be defined by (14), and denote by  $k_j$  the index of the node achieving the minimum. Then, we consider the node  $x_{k_j}$  along with its neighbors (as shown in Fig. 1), and build a least squares quadratic approximation of  $\mathcal{F}_j$  based on its values on such a stencil.

The construction of a quadratic approximation in the form

$$\begin{aligned} Q(y) &= \frac{1}{2}y^tAy - b^ty + c \\ &= \frac{1}{2}a_{11}y_1^2 + a_{12}y_1y_2 + \frac{1}{2}a_{22}y_2^2 - b_1y_1 - b_2y_2 + c, \end{aligned} \quad (30)$$

with a symmetric Hessian matrix  $A$ , requires the six parameters  $a_{11}, a_{12}, a_{22}, b_1, b_2$  and  $c$ . Under the assumption that the triangulation is acute, the stencil contains at least six nodes, and this implies that the squared residual has a unique minimum (in particular, a

zero residual if the number of nodes is precisely six, in which case  $Q$  is an interpolant). In (30) and in what follows, we neglect for simplicity of notation the dependence on the index  $j$ .

We briefly recall the adaptation of least squares approximation to the case under consideration. Let then  $\xi_l = (\xi_{l,1}, \xi_{l,2})$  for  $l = 1, \dots, M$ , denote a generic point (including  $x_{k_j}$ ) in the stencil of  $Q$ , and  $f_l$  denote the corresponding value of  $\mathcal{F}_j(k)$ , computed for  $k$  such that  $x_k = \xi_l$ . Once defined the matrix  $\Phi$  and the two vectors  $a$  and  $f$  as

$$\Phi = \begin{pmatrix} \frac{1}{2}\xi_{1,1}^2 & \xi_{1,1}\xi_{1,2} & \frac{1}{2}\xi_{1,2}^2 & -\xi_{1,1} & -\xi_{1,2} & 1 \\ \vdots & \vdots & \vdots & \vdots & \vdots & \vdots \\ \frac{1}{2}\xi_{M,1}^2 & \xi_{M,1}\xi_{M,2} & \frac{1}{2}\xi_{M,2}^2 & -\xi_{M,1} & -\xi_{M,2} & 1 \end{pmatrix}, \quad a = \begin{pmatrix} a_{11} \\ a_{12} \\ a_{22} \\ b_1 \\ b_2 \\ c \end{pmatrix}, \quad f = \begin{pmatrix} f_1 \\ \vdots \\ f_M \end{pmatrix},$$

the vector  $a$  of unknown parameters of  $Q(y)$  solves the system of normal equations

$$\Phi^t \Phi a = \Phi^t f. \quad (31)$$

Next, using the parameters obtained from (31), an easy computation gives for the minimum of  $Q(y)$  the value

$$\min_{y \in \mathbb{R}^2} Q(y) = \frac{a_{22}b_1^2 - 2a_{12}b_1b_2 + a_{11}b_2^2}{2(a_{12}^2 - a_{11}a_{22})} + c.$$

Finally, this value should replace  $\mathcal{F}_j(x_{k_j})$  in (9). In the case of Dirichlet boundary conditions, if  $x_{k_j}$  is on the boundary, then no quadratic refinement is obviously performed; if  $x_j$  is on the boundary, then the updated value  $v_j^{n+1}$  is obtained as

$$v_j^{n+1} = \min \left\{ b_j, \min_{y \in \mathbb{R}^2} Q(y) \right\}.$$

Note that the vector of unknown parameters  $a$  may be written as  $a = (\Phi^t \Phi)^{-1} \Phi^t f$ , and the pseudoinverse  $(\Phi^t \Phi)^{-1} \Phi^t$  depends on the local geometry of the grid, but not on the values in  $f$ , that is, it is a constant matrix associated to the node  $x_{k_j}$ .

**Remark 3** *Although we expect the stencil  $\{\xi_l\}_{1 \leq l \leq M}$  to be unisolvent (i.e., that  $M \geq 6$ ) and the matrix  $A$  to be positive definite, it might happen that one or both of these conditions fail to hold (for example, a Delaunay triangulation is not necessarily acute). In this case, the simplest countermeasure is to take the node value outright, without applying the quadratic refinement. This leads to a decrease of accuracy only on an expectedly minor portion of the grid.*

**Remark 4** *While this technique proves useful in the time-dependent case (as we will show in the numerical examples), its application to the stationary equation is limited to the value iteration solver, which in some sense stems from a time-dependent formulation. On the contrary, it is not clear how this refinement could be introduced in a policy iteration setting.*

## Consistency

The consistency estimate for this version of the scheme will be derived by adapting the arguments used in §2.1, and keeping the simplified 1-D setting. First, note that, given a regular function  $u$ , the error obtained by a least squares, second-order polynomial approximation of  $\mathcal{F}_j$  constructed on a fixed local stencils (of radius  $O(\Delta x)$  and with a bounded number of nodes), retains the same rate of the interpolation error, i.e.,  $O(\|\mathcal{F}_j'''\|_\infty \Delta x^3)$ . We are not aware of results in this direction (this might be a somewhat classical result), but sketch here the arguments for completeness:

1. Constructing a second order interpolating polynomial on any unisolvent subset of the stencil produces errors of order  $O(\|\mathcal{F}_j'''\|_\infty \Delta x^3)$  on the other nodes of the stencil;
2. None of these interpolators has a global residual lower than the least squares polynomial: the latter has therefore a squared residual of order (at worst)  $O(\|\mathcal{F}_j'''\|_\infty \Delta x^3)$ ;
3. Since the number of nodes of the stencil is bounded, the residual in the discrete  $\infty$ -norm is also  $O(\|\mathcal{F}_j'''\|_\infty \Delta x^3)$ ;
4. The least squares approximation appears then as an interpolation with perturbed data, where the perturbation is of the same order of the interpolation error. Then, the perturbed interpolation retains the same order of convergence of the unperturbed one.

On the other hand,

$$\mathcal{F}_j'''(y) = u_{xxx}(y, t_n) - \Delta t \frac{1}{\Delta t^3} H^{*'''}\left(\frac{x_j - y}{\Delta t}\right).$$

Again, the first term in the right-hand side is bounded, while the second, assuming that  $H^{*'''}$  is also bounded, is of order  $1/\Delta t^2$ . In this case, the difference between the minimum of  $\mathcal{F}_j$  and the minimum of its interpolate is  $O(\|H^{*'''}\|_\infty \Delta x^3)$ , and the consistency error reads

$$L(x_j, \Delta x, \Delta t) = \frac{1}{\Delta t} O\left(\frac{\Delta x^3}{\Delta t^2}\right) = O\left(\frac{\Delta x^3}{\Delta t^3}\right).$$

Therefore, the scheme is again consistent under an inverse CFL condition  $\Delta x = o(\Delta t)$ , but with a higher rate for the same  $\Delta t/\Delta x$  relationship. For example, the relationship  $\Delta t \sim \Delta x^{1/2}$  which causes the monotone scheme to be consistent with order  $O(\Delta x)$ , results in this case in a consistency rate of  $O(\Delta x^{3/2})$ .

## 6 Numerical examples

We present some numerical tests showing both the accuracy and the performance of the proposed schemes for evolutive and stationary HJ equations. Our implementation is written in C language, employing *Triangle* [11], our favorite easy-to-use library for the generation of Delaunay triangular meshes in two dimensions, and *SuiteSparse* [10], a sparse matrix

library for the solution of linear systems associated to policy improvement and quadratic refinement of the minimum search (although this choice might not be optimal in every respect). Unless otherwise stated, the numerical tests are run on a MacBook Pro equipped with an Intel Core i5 dual-core with 2.9 GHz, 8 Gb RAM and under the OS 11.7.10.

## 6.1 Evolutive case

For a first set of experiments in the time-dependent case, we consider the quadratic Hamiltonian  $H : \mathbb{R}^2 \rightarrow \mathbb{R}$  defined by  $H(p) = \frac{1}{2}|p|^2$ , choose the two initial data

$$u_{0,1}(x) = |x|, \quad u_{0,2}(x) = \min \{|x|^2 - 1, 0\}, \quad x \in \Omega,$$

where the space domain  $\Omega$  is a disc of  $\mathbb{R}^2$ , centered in the origin and with radius respectively equal to 2 in the first case and 2.5 in the second. Moreover, we fix the final time as  $T = 2$ . In this setting, it is easily proved that  $H$  and its Legendre transform coincide, and that the solutions of (3) with initial data  $u_{0,1}$  and  $u_{0,2}$  are given respectively by

$$u_1(x, t) = \begin{cases} \frac{|x|^2}{2t} & \text{if } |x| \leq t \\ |x| - \frac{t}{2} & \text{otherwise} \end{cases}, \quad u_2(x, t) = \min \left\{ \frac{|x|^2}{2t+1} - 1, 0 \right\},$$

providing classical examples of convex and semiconcave solutions (see [7]). In particular, the first solution exhibits an instantaneous regularization of the initial datum, whereas for the second one, the initial discontinuity of the gradient propagates along expanding circles. We observe that, for this final time  $T$ , the singularity remains in the interior of the domain.

In order to perform an experimental analysis for the order of convergence of the scheme (9), we fulfill all the assumptions of Theorem 1. In particular, choosing  $\Delta t = c\sqrt{\Delta x}$ , for a  $c > 0$ , where  $\Delta x$  is the maximal diameter of the elements of the triangulation, we ensure a consistency error of order  $O(\Delta x)$ . Then, denoting by  $u_{\text{ex}}$  the exact solution (for  $\text{ex} = 1, 2$ ), and by  $t_N$  the final time  $T$ , we consider relative errors in the  $L^\infty$  and  $L^1$  norm,

$$\mathcal{E}_{\Delta x}^\infty = \frac{\sup_i |u_{\text{ex}}(x_i, t_N) - v_i^N|}{\sup_i |u_{\text{ex}}(x_i, t_N)|},$$

$$\mathcal{E}_{\Delta x}^1 = \frac{\Delta x^2 \sum_i |u_{\text{ex}}(x_i, t_N) - v_i^N|}{\Delta x^2 \sum_i |u_{\text{ex}}(x_i, t_N)|}.$$

Finally, we evaluate, under grid refinement, the experimental order of convergence given by  $\text{EOC} \sim \log_2(\mathcal{E}_{\Delta x}/\mathcal{E}_{\Delta x/2})$ , for the errors in both  $L^\infty$  and  $L^1$  norms, denoted, respectively, by  $\text{EOC}^\infty$  and  $\text{EOC}^1$ .

The results for test 1 and test 2, associated with the initial conditions  $u_{0,1}$  and  $u_{0,2}$ , are shown in Tables 1–2, where, for each refinement of the grid, we also report the number of time steps  $N$ , the sizes  $|\mathcal{X}|$  and  $|\mathcal{T}|$  of the vertex and triangle lists, and the CPU time of the scheme, expressed in seconds. We set the coefficient  $C$  of the displacements (29) to  $C = 2$ .

$\Delta x$	$\Delta t$	$ \mathcal{X} $	$ \mathcal{T} $	$\mathcal{E}_{\Delta x}^1$	EOC <sup>1</sup>	$\mathcal{E}_{\Delta x}^\infty$	EOC <sup><math>\infty</math></sup>	$N$	CPUtime
0.1	0.1581	3142	6080	0.0523	-	0.0582	-	12	0.41
0.05	0.1118	12360	24329	0.025	1.09	0.031	0.90	17	3.19
0.025	0.0791	49077	97344	0.013	0.9404	0.0153	1.0225	25	27.26
0.0125	0.0559	195420	389229	0.0060	1.0896	0.0068	1.1638	35	210.25

Table 1: Test 1, experimental order of convergence for the basic version of scheme (9), with  $\Delta t = 0.5\sqrt{\Delta x}$ .

$\Delta x$	$\Delta t$	$ \mathcal{X} $	$ \mathcal{T} $	$\mathcal{E}_{\Delta x}^1$	EOC <sup>1</sup>	$\mathcal{E}_{\Delta x}^\infty$	EOC <sup><math>\infty</math></sup>	$N$	CPUtime
0.1	0.1581	3142	6080	0.0918	-	0.0917	-	12	0.43
0.05	0.1118	12360	24329	0.0415	1.1451	0.0435	1.0769	17	3.26
0.025	0.0791	49077	97344	0.0198	1.0675	0.0217	1.0024	25	26.31
0.0125	0.0559	195420	389229	0.0094	1.0770	0.01050	1.0478	35	198.99

Table 2: Test 2, experimental order of convergence for the basic version of scheme (9), with  $\Delta t = 0.5\sqrt{\Delta x}$ .

Note that the experimental order of convergence follows the theoretical consistency analysis. Moreover, test 2 allows us to show the advantages of implementing the four displacement technique. In fact, in this case, there is a large part of the domain where the solution is constant and where the minimization walks would immediately stop at a local minimum if starting from the node  $x_j$ . The displacements, if their length  $C\Delta t$  is large enough, allow the walks to bypass the singularity and find the right minimizing node.

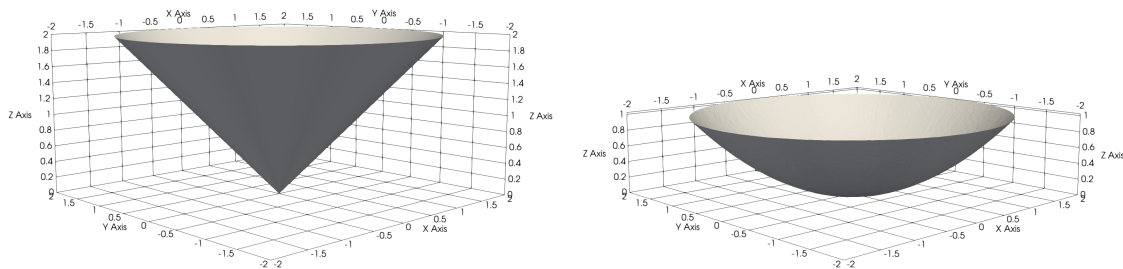


Figure 2: Test 1, numerical solution at initial time  $t = 0$  and final time  $T = 2$ , for  $\Delta x = 0.025$  and  $\Delta t = 0.5\sqrt{\Delta x} \approx 0.08$ .

## 6.2 Stationary case

In the second set of examples, we treat the static case, focusing in particular on fast solvers based on PI. As for the evolutive case, we consider the quadratic hamiltonian  $H(p) = \frac{1}{2}|p|^2$ ,

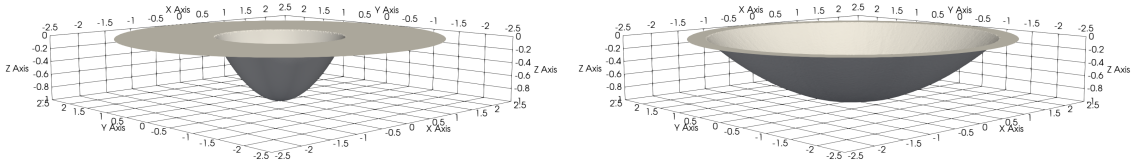


Figure 3: Test 2, numerical solution at initial time  $t = 0$  and final time  $T = 2$ , for  $\Delta x = 0.025$  and  $\Delta t = 0.5\sqrt{\Delta x} \approx 0.08$ .

we fix  $\lambda > 0$ , and we study the following two tests, where we define the function  $f$  in (7) as

$$f_3(x) = \frac{1}{2}(\lambda + 1)|x|^2, \quad f_4(x) = \frac{1}{2}(\lambda + 1) \min \{|x - (1, 0)|^2, |x + (1, 0)|^2\}.$$

Therefore, the associated solutions are

$$u_3(x) = \frac{1}{2}|x|^2, \quad u_4(x) = \frac{1}{2} \min\{|x - (1, 0)|^2, |x + (1, 0)|^2\},$$

for  $x \in \Omega \subset \mathbb{R}^2$ , where  $\Omega$  is defined as the circle centered in the origin, with radius 2.

In tables 3–4, we present the results obtained by applying the value iteration and the policy iteration schemes with rectangular integration to tests 3 and 4, with the exact solutions  $u_3$  and  $u_4$ . The value iteration starts from a constant initial guess equal to 1, and we set the fictitious time step as  $\Delta t = 0.5\Delta x^{2/3}$ , to recover a  $2/3$  consistency rate. Tables 5–6 report the corresponding results for trapezoidal integration, with  $\Delta t = 0.2\sqrt{\Delta x}$ , in order to obtain a unitary consistency rate. We set  $\lambda = 1$ , the displacements length coefficient  $C = 2$  and the stopping tolerance as  $10^{-12}$ , which is also used in the internal policy evaluation cycle of the modified PI algorithm.

In the tables,  $N$  denotes the number of iterations. The experimental convergence rate follows once more the consistency estimate, while the policy iteration solver results in a significant reduction of the CPU times (about one and a half orders of magnitude for the exact PI), without loss of accuracy in the numerical solution.

### 6.3 Quadratic refinement

The application of the quadratic refinement previously introduced is studied in the time-dependent case. We repeat test 1 and test 2 adding the minimum search on the quadratic approximation, and we collect the results in Tables 7 and 8, respectively.

We observe that the implementation of this technique results in a relevant reduction of the relative errors, at the cost of an increased CPU time. Figure 5 shows that the increase in accuracy is worth the higher complexity, by comparing the numerical errors in  $L^1$ -norm with respect to the CPU times for the scheme (9) with and without applying quadratic refinement.

$\Delta x$	$\Delta t$	$ \mathcal{X} $	$ \mathcal{T} $	$\mathcal{E}_{\Delta x}^1$	EOC <sup>1</sup>	$\mathcal{E}_{\Delta x}^\infty$	EOC <sup><math>\infty</math></sup>
0.1	0.1077	2029	3928	0.1524	-	0.1412	-
0.05	0.0678	7919	15555	0.0996	0.6131	0.0910	0.6331
0.025	0.0427	31362	62142	0.0640	0.6381	0.0580	0.6511
0.0125	0.0269	125211	249295	0.0408	0.6505	0.0364	0.6711

$\Delta x$	$N$	CPUtime
0.1	237	4.50
0.05	369	32.78
0.025	574	246.86
0.0125	893	1792.3

(a) Value iteration method

$\Delta x$	$N$	CPUtime
0.1	10	0.18
0.05	15	1.25
0.025	18	7.90
0.0125	24	45.83

(b) Exact PI method

$\Delta x$	$N$	CPUtime
0.1	10	0.39
0.05	15	2.58
0.025	18	16.20
0.0125	24	97.61

(c) Modified PI method

Table 3: Test 3, experimental order of convergence in the case of rectangular integration ( $\Delta t = 0.5\Delta x^{2/3}$ ), and comparison of the computational performances associated to the three solvers.

$\Delta x$	$\Delta t$	$ \mathcal{X} $	$ \mathcal{T} $	$\mathcal{E}_{\Delta x}^1$	EOC <sup>1</sup>	$\mathcal{E}_{\Delta x}^\infty$	EOC <sup><math>\infty</math></sup>
0.1	0.1077	2029	3928	0.1695	-	0.1318	-
0.05	0.0678	7919	15555	0.1125	0.5916	0.0851	0.6313
0.025	0.0427	31362	62142	0.0727	0.6299	0.0547	0.6381
0.0125	0.0269	125211	249295	0.0461	0.6573	0.0348	0.6515

$\Delta x$	$N$	CPUtime
0.1	237	4.53
0.05	369	32.94
0.025	574	240.83
0.0125	893	1818.48

(a) Value iteration method

$\Delta x$	$N$	CPUtime
0.1	12	0.26
0.05	14	1.22
0.025	18	7.69
0.0125	22	40.06

(b) Exact PI method

$\Delta x$	$N$	CPUtime
0.1	12	0.60
0.05	14	2.55
0.025	18	15.788
0.0125	22	87.08

(c) Modified PI method

Table 4: Test 4, experimental order of convergence in the case of rectangular integration ( $\Delta t = 0.5\Delta x^{2/3}$ ), and comparison of the computational performances associated to the three solvers.

Moreover, we observe that the quadratic refinement allows us to recover the quadratic profile of the exact solution near the origin, which is otherwise lost in the previous version of the scheme.

A comparison between the solutions obtained with the two schemes is visually reported in Figure 6, where we present the profile of the two numerical solutions for test 1, where  $\Omega$  is defined as a ball of radius 1, obtained sectioning along the plane parallel to the Z-axis passing through the points  $(-1, 0, 0)$  and  $(1, 0, 0)$ .

$\Delta x$	$\Delta t$	$ \mathcal{X} $	$ \mathcal{T} $	$\mathcal{E}_{\Delta x}^1$	EOC <sup>1</sup>	$\mathcal{E}_{\Delta x}^\infty$	EOC <sup><math>\infty</math></sup>
0.1	0.0632	2029	3928	0.1259	-	0.0940	-
0.05	0.0447	7919	15555	0.0693	0.8624	0.0477	0.9784
0.025	0.0316	31362	62142	0.0361	0.9394	0.0237	1.0116
0.0125	0.0224	125211	249295	0.0191	0.9191	0.0125	0.9182

$\Delta x$	$N$	CPUtime
0.1	394	5.04
0.05	549	33.89
0.025	766	239.34
0.0125	1067	1920.46

(a) Value iteration method

$\Delta x$	$N$	CPUtime
0.1	13	0.17
0.05	16	0.97
0.025	18	5.58
0.0125	23	41.22

(b) Exact PI method

$\Delta x$	$N$	CPUtime
0.1	13	0.36
0.05	16	2.08
0.025	18	12.30
0.0125	23	91.63

(c) Modified PI method

Table 5: Test 3, experimental order of convergence in the case of trapezoidal integration ( $\Delta t = 0.2\sqrt{\Delta x}$ ), and comparison of the computational performances associated to the three solvers.

$\Delta x$	$\Delta t$	$ \mathcal{X} $	$ \mathcal{T} $	$\mathcal{E}_{\Delta x}^1$	EOC <sup>1</sup>	$\mathcal{E}_{\Delta x}^\infty$	EOC <sup><math>\infty</math></sup>
0.1	0.0632	2029	3928	0.1718	-	0.0810	-
0.05	0.0447	7919	15555	0.0975	0.8172	0.0374	1.1152
0.025	0.0316	31362	62142	0.0526	0.8907	0.0193	0.9543
0.0125	0.0224	125211	249295	0.0271	0.9549	0.0104	0.8929

$\Delta x$	$N$	CPUtime
0.1	394	5.09
0.05	549	37.13
0.025	766	262.25
0.0125	1067	1918.26

(a) Value iteration method

$\Delta x$	$N$	CPUtime
0.1	12	0.16
0.05	16	1.23
0.025	20	6.58
0.0125	23	52.25

(b) Exact PI method

$\Delta x$	$N$	CPUtime
0.1	12	0.38
0.05	16	2.66
0.025	20	14.15
0.0125	23	129.48

(c) Modified PI method

Table 6: Test 4, experimental order of convergence in the case of trapezoidal integration ( $\Delta t = 0.2\sqrt{\Delta x}$ ) and comparison of the computational performances associated to the three solvers.

## 6.4 Parallel implementation on GPU and complex geometries

Semi-Lagrangian schemes provide a concrete example of *embarrassingly parallel* algorithms, meaning that the workload for the numerical solution of our Hamilton–Jacobi equations can be naturally split among the computational resources. Indeed, referring to Algorithm 1 for evolutive problems and to the value iteration approach for stationary problems, each node of our triangular grid can be assigned to a single thread in a parallel computation, which can perform its walks along the mesh independently, using information from the previous time step or iteration. Synchronization is needed only at the end of each iteration, but since

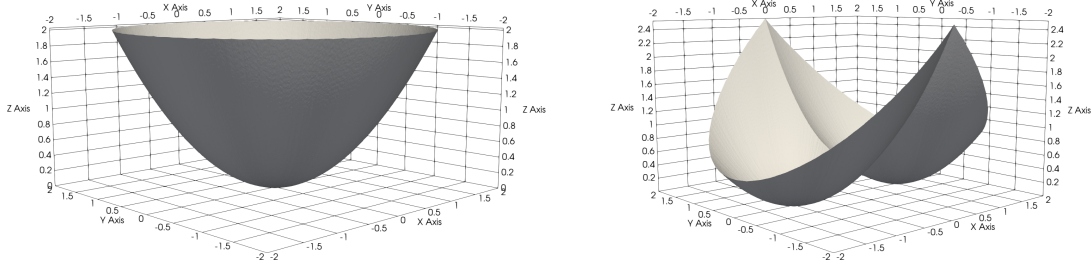


Figure 4: Tests 3–4, numerical solutions computed applying trapezoidal integration and exact policy iteration solver, for  $\Delta x = 0.0125$ ,  $\Delta t = 0.2\sqrt{\Delta x} \approx 0.02$ .

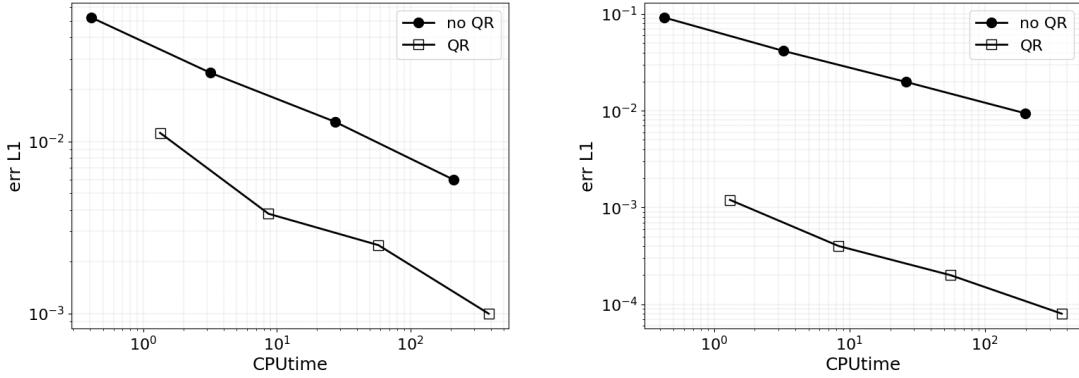


Figure 5: Test 1 (left) and test 2 (right) relative errors evolution, with respect to the times of implementation. Obtained applying scheme (9) with and without quadratic refinement, respectively for  $\Delta x = 0.1, 0.05, 0.025, 0.0125$ .

$\Delta x$	$\Delta t$	$ \mathcal{X} $	$ \mathcal{T} $	$\mathcal{E}_{\Delta x}^1$	EOC <sup>1</sup>	$\mathcal{E}_{\Delta x}^\infty$	EOC <sup><math>\infty</math></sup>	$N$	CPUtime
0.1	0.1581	3142	6080	0.0112	-	0.0234	-	12	1.34
0.05	0.1118	12360	24329	0.0038	1.5397	0.0088	1.4172	17	8.69
0.025	0.0791	49077	97344	0.0025	0.6030	0.0059	0.5788	25	57.65
0.0125	0.0559	195420	389229	0.0010	1.3899	0.0025	1.2247	35	386.67

Table 7: Test 1 experimental order of convergence for scheme (9) with quadratic refinement application, where  $\Delta t = 0.5\sqrt{\Delta x}$ .

the length of each walk is similar for each node, the amount of operations is about the same for each thread, and this clearly results in a relevant speed-up of the whole computation. Here, we implement a parallel version of the value iteration algorithm for stationary problems, written in CUDA and running on a GPU server equipped with a Nvidia H100 GPU with 94Gb Ram and 14592 CUDA cores. In the following tables, we report the results

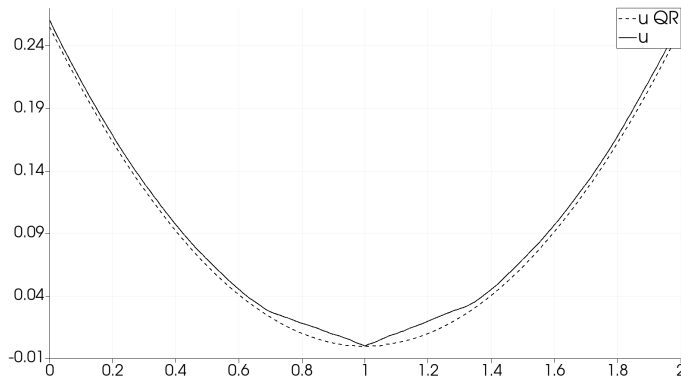


Figure 6: Sections of the numerical solutions of test 1 at final time  $T = 2$ . The numerical solutions are indicated as  $u_{QR}$  and  $u$  and are obtained applying scheme (9) with and without quadratic refinement, for  $\Delta x = 0.0125$ ,  $\Delta t = 0.5\sqrt{\Delta x} \approx 0.05$ .

$\Delta x$	$\Delta t$	$ \mathcal{X} $	$ \mathcal{T} $	$\mathcal{E}_{\Delta x}^1$	EOC <sup>1</sup>	$\mathcal{E}_{\Delta x}^\infty$	EOC <sup><math>\infty</math></sup>	$N$	CPUtime
0.1	0.1581	3142	6080	0.0012	-	0.0118	-	12	1.31
0.05	0.1118	12360	24329	0.0004	1.5727	0.0056	1.0812	17	8.32
0.025	0.0791	49077	97344	0.0002	1.1114	0.0018	1.6059	25	55.68
0.0125	0.0559	195420	389229	0.00008	1.1599	0.0014	0.3370	35	369.05

Table 8: Test 2 experimental order of convergence for scheme (9) with quadratic refinement application, where  $\Delta t = 0.5\sqrt{\Delta x}$ .

obtained for test 3 and test 4 of Section 6.2, using the same parameters and the trapezoidal quadrature rule for the approximation of the integral in the Hopf–Lax formula, showing in particular the speed-up with respect to the serial version of the code.

$\Delta x$	$N$	CPUtime	GPUtime	Speed-up
0.1	394	1.33	0.07	20x
0.05	549	9.26	0.13	68x
0.025	766	66.36	0.26	256x
0.0125	1067	478.70	1.04	462x

Table 9: Value iteration method for test 3, CPU vs GPU

We observe that the serial version of the code does not perform well even on a relatively coarse mesh (e.g.  $\Delta x = 0.0125$  corresponds to a triangulation with 125189 and 249241 triangles), while the parallel version achieves an impressive speed-up. However, a key factor limiting performance is the lack of spatial locality in unstructured grids. Unlike structured meshes, where neighbouring nodes are stored contiguously in memory, an unstructured mesh requires each node to retrieve solution values and connectivity information from global memory, leading to inefficient memory access patterns. Ideally, one

$\Delta x$	$N$	CPUtime	GPUtime	Speed-up
0.1	394	1.35	0.07	20x
0.05	549	9.38	0.13	73x
0.025	766	66.91	0.26	277x
0.0125	1067	484.76	1.02	474x

Table 10: Value iteration method for test 4, CPU vs GPU

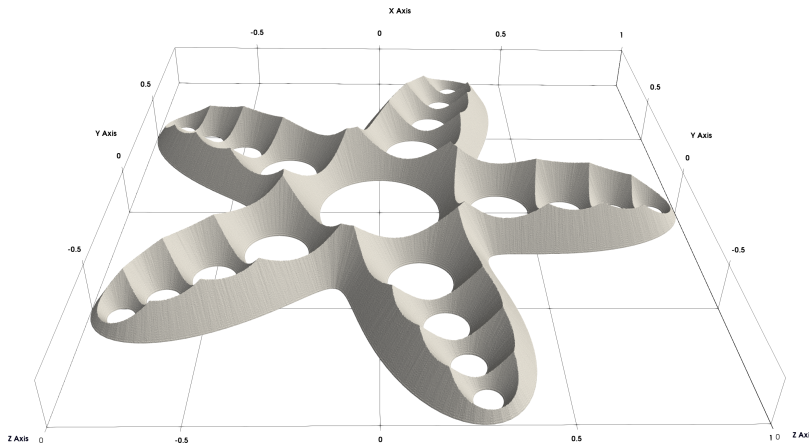


Figure 7: Numerical solution of the HJ equation (7) on a flower-shaped domain with holes.

could improve performance by grouping spatially close nodes into thread blocks so that neighbouring nodes share cached data, reducing redundant global memory accesses. The implementation of this strategy, however, falls outside the scope of the present study.

We finally report the results of an experiment showing the ability of the proposed schemes to handle complex geometries in two dimensions. We consider a flower-shaped domain with 5 petals from which some circles of different sizes have been removed. We impose homogeneous Dirichlet conditions on all the internal and external boundaries, and we consider again the case of a stationary Hamilton–Jacobi equation with quadratic Hamiltonian. Moreover, we choose  $\lambda = 1$  and we set  $f \equiv 1$  on the whole domain. In this case, it is easy to show that the solution of (7) coincides with the Kruřkov transform of the distance function from the boundary of the domain [7]. In Figure 7, we show the solution computed by the GPU version of our value iteration code. The triangular grid is composed by 330281 points and 652520 triangles, while the convergence is achieved after 37 iterations in 0.04 seconds.

## 7 Conclusions

In this paper, we introduce a numerical scheme for solving Hamilton–Jacobi equations on unstructured triangular grids using a Semi-Lagrangian approach. The key advantage of our method is that it avoids the computationally expensive interpolation step by relying solely

on nodal values, making it particularly efficient for unstructured geometries.

We provide a theoretical convergence analysis within the Barles—Souganidis framework and introduce a quadratic refinement technique to improve accuracy while maintaining computational feasibility. For stationary problems, we implemented a fast policy iteration solver, which significantly reduce computational times.

Extensive numerical tests show reliable convergence rates and robust performance even in the case of nonsmooth solutions. Additionally, we explore a GPU implementation, demonstrating substantial speed-up gains for large-scale problems.

## 8 Acknowledgements

S.C. is supported by the PNRR-MUR project *Italian Research Center on High Performance Computing, Big Data and Quantum Computing* and by the INdAM-GNCS Project code CUP E53C23001670001. R.F. and G.T. are also members of INdAM-GNCS.

## References

- [1] G. Barles and P.E. Souganidis, *Convergence of Approximation Schemes for Fully Nonlinear Second-order Equations*, *Asymp. Anal.*, **4** (1991), 271–283.
- [2] O. Bokanowski, S. Maroso, H. Zidani, *Some convergence results for Howard’s algorithm*, *SIAM Journal on Numerical Analysis* **47** (2009), 3001–3026.
- [3] A. Bouillard, E. Faou and M. Zavidovique, *Fast weak-KAM integrators for separable Hamiltonian systems*, *Math. Comp.*, **85** (2016), 85–117
- [4] S. Cacace, R. Ferretti, *Efficient implementation of characteristic-based schemes on unstructured triangular grids*, *Computational and Applied Mathematics*, **41** (2022), 1–24
- [5] M.G. Crandall, L. Tartar, *Some relations between nonexpansive and order preserving mappings*, *Proc. Amer. Math. Soc.*, **78** (1980), 385–390
- [6] M. Falcone, R. Ferretti, *Semi-Lagrangian schemes for Hamilton–Jacobi equations, discrete representation formulae and Godunov methods*, *J. of Computational Physics*, **175** (2002), 559–575.
- [7] M. Falcone and R. Ferretti, *Semi-Lagrangian approximation schemes for linear and Hamilton–Jacobi equations*, SIAM, Philadelphia, 2013.
- [8] M.L. Puterman and S.L. Brumelle, *On the convergence of policy iteration in stationary dynamic programming*, *Mathematics of Operational Research* **4** (1979), 60–69.
- [9] M.L. Puterman and M.C. Shin, *Modified policy iteration algorithms for discounted Markov decision problems*, *Management Science* **24** (1978), 1127–1137.

- [10] *SuiteSparse, A Suite of Sparse Matrix Software*,  
<https://people.engr.tamu.edu/davis/suitesparse.html>.
- [11] *Triangle, A Two-Dimensional Quality Mesh Generator and Delaunay Triangulator*,  
<https://www.cs.cmu.edu/~quake/triangle>.